Earthquake clustering controlled by shear zone interaction

Mildon, Zoë K.[1.,*], Roberts, Gerald P.[2.], Faure Walker, Joanna P.[3.], Beck, Joakim[4.], Papanikoloau, Ioannis[5.], Michetti, Alessandro M.[6.], Toda, Shinji[7.], Iezzi, Francesco[2.], Campbell, Lucy[1.], McCaffrey, Kenneth J.W.[8.], Shanks, Richard[9.] Vittori, Eutizio[10.],

1. University of Plymouth, UK
2. Birkbeck, University of London, UK
3. University College London, UK.
4. King Abdullah University of Science and Technology (KAUST), Saudi Arabia.
5. Agricultural University of Athens, Greece.
6. Università degli Studi dell'Insubria, Como, Italy.
7. Tohoku University, Sendai, Japan.
8. University of Durham, UK.
9. Scottish Universities Environmental Research Centre, East Kilbride, UK
10. Istituto Superiore per la Prevenzione e la Ricerca Ambientale, Rome, Italy.

* Corresponding author: Zoë Mildon, zoe.mildon@plymouth.ac.uk

Abstract

Earthquakes are known to cluster in time, from historical and palaeoseismic studies, but the mechanism(s) responsible for clustering, such as evolving dynamic topography, fault interaction, and strain-storage in the crust are poorly quantified, and hence not well understood. We note that differential stress values are (1) output by calculations of fault interaction, and (2) needed as input to calculate strain-rates for viscous shear zones that drive slip on overlying active faults. However, these two separate fields of geoscience have never been linked to study earthquake clustering. Here we quantify the links between these fields, and replicate observations of earthquake clustering from a 36Cl cosmogenic study of six interacting active normal faults. We derive differential stress change values from Coulomb stress transfer calculations, and use these values in a viscous flow law for dislocation creep to calculate changes in strain-rate for shear zones, and slip-rates and earthquake recurrence on overlying active faults. Our quantification of clustering, verified with observations, reveals how brittle and viscous processes in the upper and lower crust interact, driving temporal changes in slip-rate and seismic hazard.

It has long been known that earthquake recurrence is not strictly periodic, with evidence for temporal earthquake clusters lasting hundreds to thousands of years and containing several large-magnitude (M_w>6) earthquakes[1]. Currently, we lack understanding of what controls such aperiodicity. This confounds our attempts to mitigate seismic hazard, because the greater the aperiodicity, the greater the uncertainty in recurrence intervals, a vital input for time-dependent probabilistic seismic hazard assessment[2]. Boundary conditions driving the deformation are likely to be constant over the timescales of clustering of a few milennia or less[3,4], therefore it must be that the faulting process itself induces clustered activity and we investigate this herein.

An important insight comes from recent work[3], consistent with an old, but classic idea[5], that slip on brittle faults in the upper crust is driven by the slip on underlying viscous shear zones in the lower crust. The recent work revealed a correlation between strain-rates derived from measurements of slip-rates on surface fault scarps[6] and topographic elevation in the Italian Apennines extensional region, (Fig. 1). The strain-rates were averaged over a time period (15 ± 3 ka) longer than the timescale of clustered slip. The correlation takes the form of a power law, where strain-rate, $\dot{\varepsilon}$ is related to the elevation, h, in the form $\dot{\varepsilon} \propto h^n$, with n = 3.26. These authors[3], considered that h contributes to the differential stresses driving the deformation, alongside tectonic forcing, because h contributes to the vertical stress. Hence $\dot{\varepsilon} \propto h^n$ resembles the classic quartz flow law for dislocation creep in quartz shown in equation (1)[7], where, $\dot{\varepsilon}$ is strain rate, A is a material parameter, fH_2O is water fugacity, m is the water fugacity exponent, σ is the differential stress, n is the stress exponent, Q is the activation energy, R is the ideal gas constant, and T is absolute temperature.

$$\dot{\varepsilon}= AfH_2O^m\sigma^n\exp(-Q/RT) \qquad (1)$$

The power law form $\dot{\varepsilon} \propto \sigma^n$ implies that strain-rates accommodated by the brittle faults are driven by the strain-rate of the viscous deformation on underlying shear zones.

The question that arises is what would result if the differential stresses within underlying shear zones changed due to shear zone interaction? Slip on a shear zone or brittle fault will induce elastic strain in the surrounding rocks, including minerals within neighbouring mylonitic shear zones, changing the stress (Fig. 2). Values for differential stress can be calculated[8,9] via Coulomb stress calculations. These values can then be used to calculate implied changes in shear zone strain-rates using a quartz flow law[7]. These changes in strain-rate will affect the slip rates of the overlying faults; we investigate if this produces slip-rate changes of the timescale and magnitude associated with earthquake clustering.

We have no direct measurements of strain-rate changes over a few centuries or millennia for shear zones in the lower crust. However, it has been argued above that strain-rates from brittle faults reveal strain-rates in underlying shear zones[3] (Fig. 1). We measure slip-rate changes on brittle faults using *in situ* ^{36}Cl cosmogenic exposure analyses on bedrock fault scarps. This reveals that periods of rapid slip on some faults (clusters) are contemporaneous with periods of slow slip (anticlusters) on others. We input the timing and magnitude of rapid slip into stress transfer models, using the output stress changes as inputs for viscous flow calculations for dislocation creep to constrain strain-rates changes for shear zones beneath faults experiencing slow slip. Our aim is to examine whether the magnitude of strain-rate decrease is of the correct magnitude to explain the slow slip.

Cosmogenic analyses of fault scarps reveal millennial earthquake clusters

The measurements in our study come from the Italian Apennines, a region of extension since 2-3 Ma[6,10], with active normal faults deforming a pre-existing alpine fold and thrust belt[11,12]. Geodetic and seismological observations confirm extension rates of ~3 mm/yr across the Apennines[13,14].Historical and instrumental seismicity indicates that large (M_w5.5-7.0) magnitude normal faulting earthquakes occur[15,16] and produce surface carbonate fault scarps[6,17–19] (Fig. 1e). The surface fault scarps have been preserved since the demise of the last glacial maximum (LGM, 15 ±3 ka), due to a reduction in erosion rates relative to throw rates[20] (Fig. 1). These scarps have been studied with *in situ* ^{36}Cl cosmogenic exposure analyses, confirming the post-LGM slope stabilisation age and fault slip rate histories that are variable during the Holocene[21,22]. In places, dense ^{36}Cl sampling has revealed correlation of high slip-rate events with the timing of damaging earthquakes that affected Rome[23].

We focus on a single normal fault in the central Apennines because this fault recently ruptured after an anomalously long elapsed time since the last earthquake. The Mt. Vettore fault ruptured to the surface in the August-October 2016 sequence, which included Mw 6.2, 6.1 and 6.6 earthquakes (Fig. 1e). Paleoseismological studies suggest that before 2016, this SW-dipping active normal fault had not ruptured to the surface for several thousand years, with suggestions of the elapsed time ranging between 1316-4155 years BP[24], and 6446 +1330/-2660 years BP[25]. Interestingly, during this period, five other nearby faults have ruptured to the surface in damaging historical earthquakes with elapsed times of less than a few hundred years, (1349 AD, Fiamignano fault; 1639 AD, Laga fault; 1703 AD, Norcia and Barete faults; 1997 AD Mt Le Scalette fault; late Holocene, Leonessa fault), revealed by historical accounts, paleoseismic studies and ^{36}Cl studies[23,26–32]. A pattern emerges where one fault has not slipped, whilst its neighbours have slipped in the same time period. It is this intriguing observation that motivated our study.

We sampled the six faults for ^{36}Cl cosmogenic analyses prior to the 2016 earthquakes, sampling up the fault plane and within shallow (<~1m) trenches parallel to the slip-vector. We constrained the sample sites with geological mapping and topographic surveys. These data confirm the exposed fault scarps are formed solely due to tectonic slip and not erosional/depositional processes. We statistically inferred the slip implied by the ^{36}Cl data using a Bayesian Markov chain Monte Carlo (MCMC) approach[23]. The results show evidence of slip-rate changes that imply temporal earthquake clustering (Fig. 3). We note that rapid slip occurred synchronously on the SW and NE flank of the Apennines (e.g. compare slip in the last few thousand years on the Laga and Fiamignano faults). This rules out the hypothesis that activity migrates, producing clustering, due to least-work constraints imposed by spatial changes in dynamic topography[22].

We have four key observations from our statistical modelling of the ^{36}Cl data that help to reveal the cause of the slip-rate changes (Fig. 3): (1) the slip-rate on the Mt. Vettore fault slows at ~4 ka; (2) the other faults accelerated, starting at ~3.5 ka; (3) prior to ~4 ka, the Mt. Vettore fault underwent a high slip-rate phase relative to its slip-rate averaged since ~17.5 ka; (4) prior to ~3.5 ka, the other faults had slip-rates that were relatively low compared their 15 ±3 kyrs average slip rate. Our observations are consistent with existing paleoseismic observations[25,28]. The question that arises is whether the underlying viscous shear zones were also involved in the interaction, slowing or accelerating in tandem with their overlying brittle faults.

Calculating the effect of fault interaction on stress transfer and strain rate changes

To quantify interactions between the faults and the viscous shear zones, we extracted the amount of slip on each fault in the time period from ~3.5 ka to 2015 AD, and prior to ~3.5 ka. We modelled the Coulomb stress transfer (CST)[9] implied by the amount of slip derived from the ^{36}Cl modelling in each time period (e.g. Fig. 3). We calculate CST on neighbouring faults and shear zones (so-called receiver faults/shear zones) (Fig. 4), and convert to differential stress[8] for shear zones. We concentrate our analysis on the Mt. Vettore and Leonessa faults, because these faults are located centrally in the study area and receive stress from slip on both along-strike and across-strike faults that we can constrain with ^{36}Cl and paleoseismic data[28,33] (Fig. 3). The calculations reveal stress-loading histories during temporal earthquake anticlusters, on the Mt. Vettore and Leonessa faults and underlying shear zones (Fig. 4). We discuss the results for faults and shear zones separately.

For faults, we do not find a consistent pattern of increasing or decreasing CST during anticlusters. For the Mt. Vettore fault, we find that the CST from neighbouring fault slip became mostly positive during its quiescence from ~3.5 ka to present (Fig. 4aii), before it ruptured in 2016[34]. An earthquake after a relatively-long elapsed time is perhaps intuitively expected because faults will be loaded through time by far-field tectonic forces[35], and CST may positively load the fault[36]. However this intuitive view breaks down for the Leonessa fault, because the CST became increasingly negative during its low slip-rate time period from 17 ka to ~3.5 ka (Fig. 4iv). Despite the negative CST, the Leonessa fault did not cease activity, with ^{36}Cl data indicating an accumulation of 6.5 m slip between 3.5 to present, with historical constraints narrowing this to 3.5 to 0.7 ka, proving it is a Holocene active fault[31]. Overall, it appears that CST on brittle faults does not directly explain why brittle faults experience anticlusters and then rupture, as the loading can be positive or negative due to fault interaction.

For shear zones we find a consistent pattern of stress loading during anticlusters. During the two anticlusters we study, the magnitudes of differential stress change for shear zones are in the range of -2.8 to -4.0 MPa. This is significant given that we expect the differential stress in shear zones to be only ~10 MPa, and essentially constant over the ~15-24 km depth range, from investigations of exhumed extensional shear zones[37] (Figs. 4ai and 4iii). The Mt. Vettore shear zone experienced a stress reduction of up to -2.8 MPa between 3.5 ka and 2015 AD. The Leonessa shear zone experienced a stress reduction of up to -4.0 MPa between 17 and 3.5 ka. This observation that differential stress change was negative when both overlying faults had very low slip-rates (anticlusters) prompted us to investigate whether the magnitudes of differential stress reduction generate strain-rate changes comparable to our observations from ^{36}Cl.

To calculate the implied change in strain-rate for each shear zone within the two anticlusters, we input the reductions of differential stress into Equation 1, using appropriate values for other variables[7]. Assuming the patch with the largest stress decrease is the rate-limiting element, it is implied that strain-rates would have decreased from 1.5×10^{-16} to 5.0×10^{-17} on the Mt. Vettore shear zone between 3.5 ka and 2015 AD, whilst for the Leonessa shear zone strain-rate would have been decreased from 1.5×10^{-16} to 2.8×10^{-17} between 17-3.5 ka (Figs. 4a,b). Thus, both shear zones were still active during periods of earthquake quiescence, albeit with reduced strain-rates. Therefore earthquake ruptures on the overlying faults at the end of both anticlusters suggests that the impact of stress changes on the brittle faults, either positive or negative, is overwhelmed through time by slip and loading associated with the underlying viscous shear zones.

To compare the effect of the implied strain-rate changes with our ^{36}Cl measurements of the natural system, we converted the strain-rates in the shear zones into implied slip-rates on the overlying brittle faults, and compared them with the observed slip-rates (Figs. 3 and 4). We used the slip measured over the total time period constrained with ^{36}Cl as a measure of the stable long-term slip-rate[3]. We compare these long-term slip-rates with slip-rates during clusters/anticlusters constrained by the ^{36}Cl data. This allows us to calculate slip-rate enhancement factors (SRE) that describe how much the slip-rates over millennia were enhanced (SRE >1) or impeded (SRE <1) compared to the long-term slip-rates (Fig. 4c). SRE values range between <1 to >4 in both the measured and implied slip-rate datasets. We find that the implied slip-rate histories resemble those derived from ^{36}Cl (Fig. 4ci), as does implied SRE compared to measured SRE (Fig. 4cii; $R^2 = 0.985$). This implies that our novel approach outlined herein is able to explain key slip-rate observations from the natural system, providing insight into the processes that drive earthquake clustering and anticlustering.

Implications for seismic hazard and continental extension

Earthquake clustering confounds our ability to mitigate seismic hazard because the greater the aperiodicity in recurrence intervals in fault-based time-dependent hazard assessments, the greater the uncertainty that will need to be communicated probabilistically with regard to recurrence of expected ground accelerations within stated time periods[2]. Greater uncertainty may lead to reluctance with regard to implementing costly mitigation strategies. One approach to explain the aperiodicity is to suggest that the processes that control slip are multiple, complex, interacting, and difficult to quantify, and the system may be considered as approaching random behavior[38]. However, the key implication herein is that, instead, earthquake clustering appears to have a dominant, quantifiable cause, and is therefore not random. Our results suggest that viscous shear zones slow or accelerate due to changes in differential stress produced by slip on nearby viscous shear zones and brittle faults. Our results appear to rule out the notions that upper crustal brittle fault interaction[39], or least-work constraints imposed by dynamic topography[21] are the sole controls responsible for earthquake clustering. Our interpretation, where shear zone strain-rates change due to stress transfer altering the differential stress, may be linked to suggestions that tectonic strain is stored during anticlusters[40,41], and/or may be linked to the mechanism by which microstructural evolution leads to shear-zone strengthening during anticlusters if this process occurs[42]. Clearly, more work is needed, but the links we have made between geomorphic offsets, cosmogenic dating of faults scarps, calculations of stress transfer, and viscous flow laws, provide important new insights into seismic hazard that go beyond what can be achieved by simply studying instrumental seismicity. In particular, our results suggest that we should expect slip-rate changes through time on the timescale of earthquake clustering, as these are the natural consequence of fault and shear zone interactions. These slip-rate changes will alter earthquake recurrence rates and should be included in seismic hazard calculations. This approach warrants further study and we suggest that an independent test of our model will require calculations of stress change due to slip within time periods with precise time constraints such as we provide herein. Such studies will improve our ability to use values of slip-rate variability and aperiodic earthquake recurrence within fault-based probabilistic seismic hazard assessments[42].

Acknowledgements

This work was funded by NERC Standard Grant NE/I024127/1, NERC Large Grant NE/J016497/1, NERC Standard Grant NE/E01545X/1, NERC Studentship NE/L501700/1, NERC Urgency Grant NE/P01660X/1 (EEFIT Reconnaissance Mission to the Amatrice, Italy, 24/09/2016 Earthquake), Japan Society for the Promotion of Science (JSPS) Short Term Fellowship PE15776, the Jeremy Willson Charitable Trust, Geological Society Mike Coward fieldwork fund, and GBSF (Great

Britain Saskawa Foundation) grant 4602. We thank Laura Gregory for discussions, participation in fieldwork, chemical analyses and preparation of the ^{36}Cl samples. We thank Patience Cowie for many discussions and ideas that helped to lead us to this study. We thank Andrew Watson and Luke Wedmore for their assistance in the field during sampling. We thank Richard Phillips for setting up the cosmogenic lab at the University of Leeds where the sample preparation took place. The cosmogenic data is published online in a repository and is freely available for download at https://www.bgs.ac.uk/services/ngdc/accessions/index.html#item128345.

Contributions

ZM performed all the Coulomb stress modelling, helped to locate, sample and process some of the ^{36}Cl data, helped to develop our approach to fault/shear-zone interactions and use of the quartz flow law, and co-wrote the manuscript, providing diagrams and supplements. GR provided background knowledge of the regional geology, seismicity and geodesy, helped to locate and sample ^{36}Cl sites, overseeing field constraints on all sites, modelled the ^{36}Cl data, helped to develop our approach to fault/shear-zone interactions and use of the quartz flow law, and our comments on seismic hazard, and co-wrote the manuscript, providing diagrams and supplements. JFW calculated strain rates for the region, helped with fieldwork, and helped to develop our approach to fault/shear-zone interactions, quartz flow modelling and our comments on seismic hazard. JB led development of our approach to modelling slip histories from the ^{36}Cl data, and helped with some of the modelling. IP assisted with site sampling and characterization, provided knowledge of the local geology, and helped develop our comments on seismic hazard. AM assisted with site sampling and characterization and contributed knowledge on the local geology, seismicity and geodesy, and advised on seismic hazard. ST helped to determine how to calculate differential stress from Coulomb stress. FI helped with discussions on interaction, seismic hazard and local geology, seismicity and geodesy. LC contributed to understanding of shear zone deformation, quartz flow laws and differential stress. KM helped with site characterisation and tectonic interpretations. RS ran the AMS for the ^{36}Cl samples and helped with some field sampling. EV advised on local geology, seismicity, geodesy, and seismic hazard. All authors contributed to editing the manuscript.

Methods

Inversion of slip histories from ^{36}Cl cosmogenic dating: Sites for cosmogenic sampling from limestone bedrock faults planes are carefully selected to ensure that the scarps are formed solely by tectonic exhumation (see Supplementary Material 1 which describes the characteristics of each sample site). A good site will have parallel hanging wall/footwall intersections with the fault plane, a smooth lower slope on the hanging wall devoid of erosional or depositional features, and will avoid active gullies or other erosional features present on the footwall or fault plane. 15 x 5 x 2.5 cm sized samples of fault plane were taken parallel to the slip vector measured from frictional wear striations. These samples were prepared following the approach of refs.[22,43] and were analysed with AMS to determine the concentrations of ^{36}Cl in each sample. The concentration of ^{36}Cl increases up the fault plane as the length of time of exposure increases. We used the Bayesian MCMC code of ref.[23] to inverse model the slip history from measured concentrations of ^{36}Cl (results of the modelling are shown in Supplementary Material 2). This code searches for the probability distribution of the slip history conditioned on the measured data, and as an outcome identifies a slip history of best least-squares fit, while allowing a high flexibility of the magnitude and timings of slip events, uncertainties in the density of the colluvium and ^{36}Cl production factors, and timing of ^{36}Cl initial production. We have also iterated inputs, such as the total slip across the scarps (Supplementary Material 3), and find that the strain-rate and SRE results are relatively insensitive to uncertainty in these values. We also show that sample spacings on the fault planes we achieved are adequate to resolve the slip-rate changes we claim. We do this by progressively degrading the dense sampling for the Fiamignano fault to a point where two well-constrained historical earthquake sequences resolvable with the full data disappear (Supplementary Material 4). The full approach to the statistical modelling of slip histories using the ^{36}Cl data is described in [23].

Modelling Coulomb stress changes: Non-planar strike-variable fault geometries are built as a series of rectangular elements[44] that are ~1km^2. The geometry of the faults is based on extensive field data collected from limestone bedrock fault scarps in the central Apennines[45–51]. These strike-variable fault geometries are utilized in Coulomb 3.4[36] to model Coulomb stress changes associated with earthquakes and slip on underlying shear zones. The brittle ductile transition is assumed to be at 15 km depth and shear zones are assumed to extend from 15 – 24 km depth[3]. For each fault, a characteristic earthquake magnitude is calculated using the relationship between fault area and magnitude[52]. A simple concentric slip distribution is calculated, assuming 40% of the maximum slip at depth reaches the surface, and the maximum slip is iterated to match the earthquake magnitude. The 40% assumption is based on iterating this value to closely match the ratios between (1) average subsurface displacement and maximum surface displacement and (2) average subsurface displacement and average surface displacement[52] (0.76 and 1.32 modal values respectively). It is not possible to exactly match the modal values, the values reported herein are within the variability reported[52]. The values used to calculate the characteristic magnitude are given in Table 1.

Fault name	Fault length (km)	Fault dip (•)	Downdip length (km)	Fault area (km^2)	M$_{max}$	ASS/ MS	ASS/ AS	Max. slip (m)	Slip @ cosmo site (m)
Barete	19.7	42	22.4	441.6	6.66	0.71	1.41	2.40	0.64
Fiamignano	30.7	53	18.8	576.6	6.78	0.70	1.39	3.10	1.22
Laga	30.2	53	18.8	567.2	6.77	0.72	1.39	3.00	1.16
Leonessa	14.3	62	17.0	242.9	6.41	0.69	1.38	2.00	0.43
Mt Le Scalette	18.0	62	17.0	305.8	6.51	0.68	1.40	2.40	0.83
Vettore	32.9	63	17.0	558.9	6.76	0.69	1.32	3.20	1.13

Table 1 – Parameters used to calculate the characteristic earthquake magnitude modelled on the faults discussed and to constrain the proportion of slip that occurs at the surface compared to depth. The concentric slip distribution assumes a symmetrical triangular surface slip distribution. ASS/MS = Average SubSurface displacement/Mean Surface displacement. AS/MS = Average subsurface displacement/Average Surface displacement

The contribution of each structure to the CST on the brittle faults is shown in Supplementary Material 5. The annual magnitude of slip on underlying shear zones is calculated from the Holocene throw profiles measured through fieldwork, as these are suggested to be equivilent[21].

Calculating differential stress changes: Coulomb stress changes are defined as $\Delta\sigma_{CST} = \Delta\tau + \mu\Delta\sigma_n$[53], where $\Delta\tau$ is the change in shear stress, μ is the coefficient of friction (herein 0.4 is used[44]) and $\Delta\sigma_n$ is the change in normal stress. The shear stress can be defined as $\tau = \frac{1}{2}(\sigma_1 - \sigma_3)sin2\beta$ [8] where $(\sigma_1 - \sigma_3)$ is the differential stress and β is the angle between σ_1 and the fault plane. In the central Apennines, normal faulting is dominant and therefore we assume σ_1 is vertical. Therefore $\beta = 90 - \theta$ where θ is the dip of the fault. We have calculated the differential stress using the equations above and the shear stress calculated from Coulomb 3.4. The differential stress is calculated for each 1 x 1km rectangular fault patch for the brittle and ductile portions of the faults. The conversion between sig_reverse (direct output from Coulomb 3.4) and differential stress is given in Supplementary Material 5.

Calculating change in strain-rates: Viscous deformation via dislocation creep, derived from laboratory experiments, is given by the following equation[7]: $\dot{\varepsilon} = \mathrm{A}\mathrm{f}_{\mathrm{H_2O}}^{\mathrm{m}}\sigma^{\mathrm{n}}\mathrm{e}^{\frac{-\mathrm{Q}}{\mathrm{RT}}}$, where $\dot{\varepsilon}$ is the strain rate, *A* is a material parameter, $\mathrm{f}_{\mathrm{H_2O}}^{\mathrm{m}}$ is the water fugacity, σ is the differential stress, *n* is the stress exponent, *Q* is the activation energy, *R* is the ideal gas constant and *T* is the temperature. For the dislocation creep of wet quartz[7], the following constant values are used: A = 6.31e-12 MPa/s, Q = 35kJ/mol[7], R = 8.31 $\mathrm{m^2\ kgs^{-2}K^{-1}mol^{-1}}$, *n*=3.26[3], T = 710K / 440 °C[3], $f_{H_2O}^{m}$= 110 MPa (calculated given T = 440 °C[3] and pressure = 0.4GPa @15 km depth using the online fugacity calculator[54,55]). We choose this flow law for the following reasons: (a) dislocation creep mechanisms are common in natural quartz-bearing shear zones that dominate lower continental crust at the temperature and pressure range ascribed here[37]; (b) the chosen flow law[7] considers the effect of water fugacity and is relatively well-constrained via comparison to naturally deformed rocks; (c) the use of this flow law allows consistency with previous studies in this region from which we take the stress exponent[3]. We implement the calculations using Supplementary Material 6. Although the published flow law[7] uses n = 4, we substitute n = 3.26 as derived for the Apennines region[3]. This has little effect on the resulting strain rate, which is the same order of magnitude at 10 MPa differential stress. The absolute value of differential stress is taken to be 10 MPa as values across this depth range are thought to be relatively uniform[37]. The change in differential stress is calculated from the Coulomb stress modelling. Sensitivity to the chosen values for differential stress and stress exponent are shown in Supplementary Material 7. Sensitivity to overestimating or underestimating the amount of slip across the scarps for strain-rates is shown in Supplementary Material 8. We converted the implied strain-rates for the shear zones into implied slip-rates and slip-rate changes for the overlying brittle faults by using (1) the ratio of strain-rates before and after the rate changes, and (2) the slip-rates over the entire observation period constrained in terms of timing from ^{36}Cl, and offset using scarp profiles at the surface (Supplementary Material 6). These long-term slip-rates were multiplied by the ratio of strain-rates before and after the rate changes, and amounts of slip were recovered before and after slip-rate changes, by multiplying the ratio-modified slip-rates by the time periods in question. We used these values to compare measured and implied SRE values. We also show that implied earthquake recurrence intervals for 1 m slip events (typical of the region) are of reasonable duration (a few millennia from paleoseismology[28,29,33]), given the values we input into the quartz flow law, by calculating the recurrence intervals for 1m heave events, given that we can measure the across strike distance for the region, and can calculate heave rates before and after strain-rate changes assuming faults and shear zones dip at 45°. Supplementary Material 6 shows that recurrence intervals for 1 m heave events change from ~3.6 kyrs to ~10-19 kyrs during anticlusters, comparable in terms of order of magnitude to values from paleoseismology.

References

1. Sieh, K. *et al.* A more precise chronology of earthquakes produced by the San Andreas Fault in southern California. *J. Geophys. Res. Solid Earth1* **94,** 603–623 (1989).
2. Pace, B. *et al.* Layered seismogenic source model and probabilistic seismic-hazard analyses in central Italy. *Bull. Seismol. Soc. Am.* **96,** 107–132 (2006).
3. Cowie, P. A. *et al.* Viscous roots of active seismogenic faults revealed by geologic slip rate variations. *Nat. Geosci.* **6,** 1036–1040 (2013).
4. Copley, A. *et al.* Unexpected earthquake hazard revealed by Holocene rupture on the Kenchreai Fault (central Greece): Implications for weak sub-fault shear zones. *Earth Planet. Sci. Lett.* **486,** 141–154 (2018).
5. Sibson, R. H. Fault rocks and fault mechanisms. *J. Geol. Soc. London.* **133,** 191–213 (1977).
6. Roberts, G. P. & Michetti, A. M. Spatial and temporal variations in growth rates along active normal fault systems: An example from The Lazio-Abruzzo Apennines, central Italy. *J. Struct. Geol.* **26,** 339–376 (2004).
7. Hirth, G. *et al.* An evaluation of quartzite flow laws based on comparisons between experimentally and naturally deformed rocks. *Int. J. Earth Sci.* 77–87 (2001). doi:10.1007/s005310000152
8. King, G. C. P. *et al.* Static stress changes and the triggering of earthquakes. *Bull. Seismol. Soc. Am.* **84,** 935–953 (1994).
9. Mildon, Z. K. *et al.* Coulomb pre-stress and fault bends are ignored yet vital factors for earthquake triggering. *Nat. Commun.* 1–9 (2019). doi:10.31223/osf.io/pt829

10. Cavinato, G. P. & De Celles, P. G. Extensional basins in the tectonically bimodal central Apennines fold-thrust belt, Italy: Response to corner flow above a subducting slab in retrograde motion. *Geology* **27,** 955–958 (1999).
11. Nijman, W. Tectonics of the Velino-Sirente area, Abruzzi, Central Italy, K. *Koninkl. Nederl. Akad. van Wet.* 156–184 (1971).
12. Doglioni, C. Some remarks on the origin of foredeeps. *Tectonophysics* **228,** 1–20 (1993).
13. D'Agostino, N. *et al.* Contemporary crustal extension in the Umbria-Marche Apennines from regional CGPS networks and comparison between geodetic and seismic deformation. *Tectonophysics* **476,** 3–12 (2009).
14. Selvaggi, G. Spatial distribution of horizontal seismic strain in the Apennines from historical earthquakes. *Ann. di Geofis.* **41,** (1998).
15. Anderson, H. & Jackson, J. Active tectonics of the Adriatic region. *Geophys. J. R. Astron. Soc.* **91,** (1987).
16. Chiaraluce, L. *et al.* The 2016 Central Italy Seismic Sequence: A First Look at the Mainshocks, Aftershocks, and Source Models. *Seismol. Res. Lett.* **88,** 757–771 (2017).
17. Galli, P. *et al.* Twenty years of paleoseismology in Italy. *Earth-Science Rev.* **88,** 89–117 (2008).
18. Civico, R. *et al.* Surface ruptures following the 30 October 2016 Mw 6.5 Norcia earthquake, central Italy. *J. Maps* **14,** (2018).
19. Alessio, G. *et al.* Evidence for Surface rupture associated with the Mw 6.3 L'Aquila earthquake sequence of April 2009 (central Italy). *Terra Nov.* **22,** 43–51 (2010).
20. Tucker, G. E. *et al.* Geomorphic significance of postglacial bedrock scarps on normal-fault footwalls. *J. Geophys. Res. Earth Surf.* **116,** 1–14 (2011).
21. Palumbo, L. *et al.* Slip history of the Magnola fault (Apennines, Central Italy) from36Cl surface exposure dating: Evidence for strong earthquakes over the Holocene. *Earth Planet. Sci. Lett.* **225,** 163–176 (2004).
22. Cowie, P. A. *et al.* Orogen-scale uplift in the central Italian Apennines drives episodic behaviour of earthquake faults. *Sci. Rep.* **7,** 1–10 (2017).
23. Beck, J. *et al.* Bayesian earthquake dating and seismic hazard assessment using chlorine-36 measurements (BED v1). *Geosci. Model Dev. Discuss.* **2018,** 1–24 (2018).
24. Galadini, F. & Galli, P. Paleoseismology of silent faults in the Central Apennines (Italy): The Mt. Vettore and Laga Mts. faults. *Ann. Geophys.* **46,** 815–836 (2003).

25. Cinti, F. R. *et al.* 22-kyr-Long Record of Surface Faulting Along the Source of the 30 October 2016 Earthquake (Central Apennines, Italy), From Integrated Paleoseismic Data Sets. *J. Geophys. Res. Solid Earth* 1–28 (2019). doi:10.1029/2019jb017757
26. Guerrieri, L. *et al.* Evoluzione recente dea paesaggio e dissesto geologico-idraulico: primo risultati in un'area campione dell'Appennino Centrale (valle del Salto–Rieti). *Boll. della Soc. Geol. Ital.* **57,** 453–461 (2002).
27. Boncio, P. *et al.* Defining a model of 3D seismodenic sources for Seismic Hazard Assessment applications: The case of central Apennines (Italy). *J. Seism.* **8,** 407–425 (2004).
28. Galli, P. *et al.* Holocene paleoseismology of the Norcia fault system (Central Italy). *Tectonophysics* **745,** 154–169 (2018).
29. Galli, P. A. C. *et al.* Palaeoseismology of the L'Aquila faults (central Italy, 2009, Mw6.3 earthquake): Implications for active fault linkage. *Geophys. J. Int.* **187,** 1119–1134 (2011).
30. Vittori, E. *et al.* Ground effects and surface faulting in the September-October 1997 Umbria-Marche (Central Italy) seismic sequence. *J. Geodyn.* **29,** 535–564 (2000).
31. Michetti, A. M. & Serva, L. New data on the seismotectonic potential of the Leonessa Fault area (Rieti, central Italy). *Rend. della Soc. Geol. Ital.* **13,** 37–46 (1990).
32. Blumetti, A. M. Neotectonic investigation of evidence of paleoseismicity in the epicentral area of the January-February 1703, central Italy, earthquakes. *Perspect. Paleoseismology* **6,** 83–100 (1995).
33. Cinti, F. R. *et al.* Evidence for Surface Faulting Earthquakes on the Montereale Fault System (Abruzzi Apennines, Central Italy). *Tectonics* (2018). doi:10.1029/2017TC004780
34. Mildon, Z. K. *et al.* Coulomb stress transfer and fault interaction over millennia on non-planar active normal faults: the Mw 6.5-5.0 seismic sequence of 2016-2017, central Italy. *Geophys. J. Int.* **210,** (2017).
35. Reid, H. F. The mechanics of the earthquake. *Calif. Earthq. April 1906* **18,** 192 (1910).
36. Toda, S. *et al.* Forecasting the evolution of seismicity in southern California: Animations built on earthquake stress transfer. *J. Geophys. Res. Solid Earth* **110,** 1–17 (2005).
37. Behr, W. M. & Platt, J. P. A naturally constrained stress profile through the middle crust in an extensional terrane. *Earth Planet. Sci. Lett.* **303,** 181–192

(2011).

38. Main, I. G. Earthquakes as Critical Phenomena: Implications for Probabilistic Seismic Hazard Analysis. *Bull. Seismol. Soc. Am.* **85,** 1299–1308 (1995).

39. Pace, B. *et al.* Do static stress changes of a moderate-magnitude earthquake significantly modify the regional seismic hazard? Hints from the L'Aquila 2009 normal-faulting earthquake (Mw 6.3, central Italy). *Terra Nov.* **26,** 430–439 (2014).

40. Dolan, J. F. *et al.* Extreme multi-millennial slip rate variations on the Garlock fault, California: Strain super-cycles, potentially time-variable fault strength, and implications for system-level earthquake occurrence. *Earth Planet. Sci. Lett.* **446,** 123–136 (2016).

41. Fay, N. & Humphreys, E. Dynamics of the Salton block: Absolute fault strength and crust-mantle coupling in Southern California. *Geology* **34,** 261–264 (2006).

42. Dolan, J. F. *et al.* Long-range and long-term fault interactions in Southern California. *Geology* **35,** 855–858 (2007).

43. Stone, J. O. *et al.* Cosmogenic chlorine-36 from calcium spallation. *Geochim. Cosmochim. Acta* **60,** 679–692 (1996).

44. Mildon, Z. K. *et al.* Evaluating models of Coulomb stress transfer: Is variable fault geometry important? *Geophys. Res. Lett.* **43,** (2016).

45. Roberts, G. P. Visualisation of active normal fault scarps in the Apennines, Italy: a key to assessment of tectonic strain release and earthquake rupture. *J. Virtual Explor.* **29,** (2008).

46. Faure Walker, J. P. *et al.* Comparison of earthquake strains over 10^{2} and 10^{4} year timescales: Insights into variability in the seismic cycle in the central Apennines, Italy. *J. Geophys. Res.* **115,** B10418 (2010).

47. Morewood, N. C. & Roberts, G. P. The geometry, kinematics and rates of deformation within an en echelon normal fault segment boundary, central Italy. *J. Struct. Geol.* **22,** 1027–1047 (2000).

48. Roberts, G. P. & Michetti, A. M. Spatial and temporal variations in growth rates along active normal fault systems: an example from The Lazio–Abruzzo Apennines, central Italy. *J. Struct. Geol.* **26,** 339–376 (2004).

49. Wilkinson, M. *et al.* Slip distributions on active normal faults measured from LiDAR and field mapping of geomorphic offsets: An example from L'Aquila, Italy, and implications for modelling seismic moment release. *Geomorphology* **237,** (2015).

50. Mildon, Z. K. *et al.* Active normal faulting during the 1997 seismic sequence in

Colfiorito, Umbria: Did slip propagate to the surface? *J. Struct. Geol.* **91,** 102–113 (2016).

51. Papanikolaou, I. D. *et al.* Fault scarps and deformation rates in Lazio–Abruzzo, Central Italy: Comparison between geological fault slip-rate and GPS data. *Tectonophysics* **408,** 147–176 (2005).
52. Wells, D. L. & Coppersmith, K. J. New empirical relationships among magnitude, rupture length, rupture width, rupture area, and surface displacement. *Bull. Seismol. Soc. Am.* **84,** 974–1002 (1994).
53. Harris, R. A. & Simpson, R. W. Changes in static stress on southern California faults after the 1992 Landers earthquake. *Nature* **360,** 251–254 (1992).
54. Withers, T. Fugacity calculator. (2019). Available at: https://www.esci.umn.edu/people/researchers/withe012/fugacity.htm. (Accessed: 11th March 2019)
55. Pitzer, K. S. & Sterner, S. M. Equations of state valid continuously from zero to extreme pressures for H2O and CO2. *J. Chem. Phys.* **101,** 3111–3116 (1994).
56. Faure Walker, J. P. *et al.* Relationship between topography, rates of extension and mantle dynamics in the actively-extending Italian Apennines. *Earth Planet. Sci. Lett.* **325–326,** 76–84 (2012).

Figures

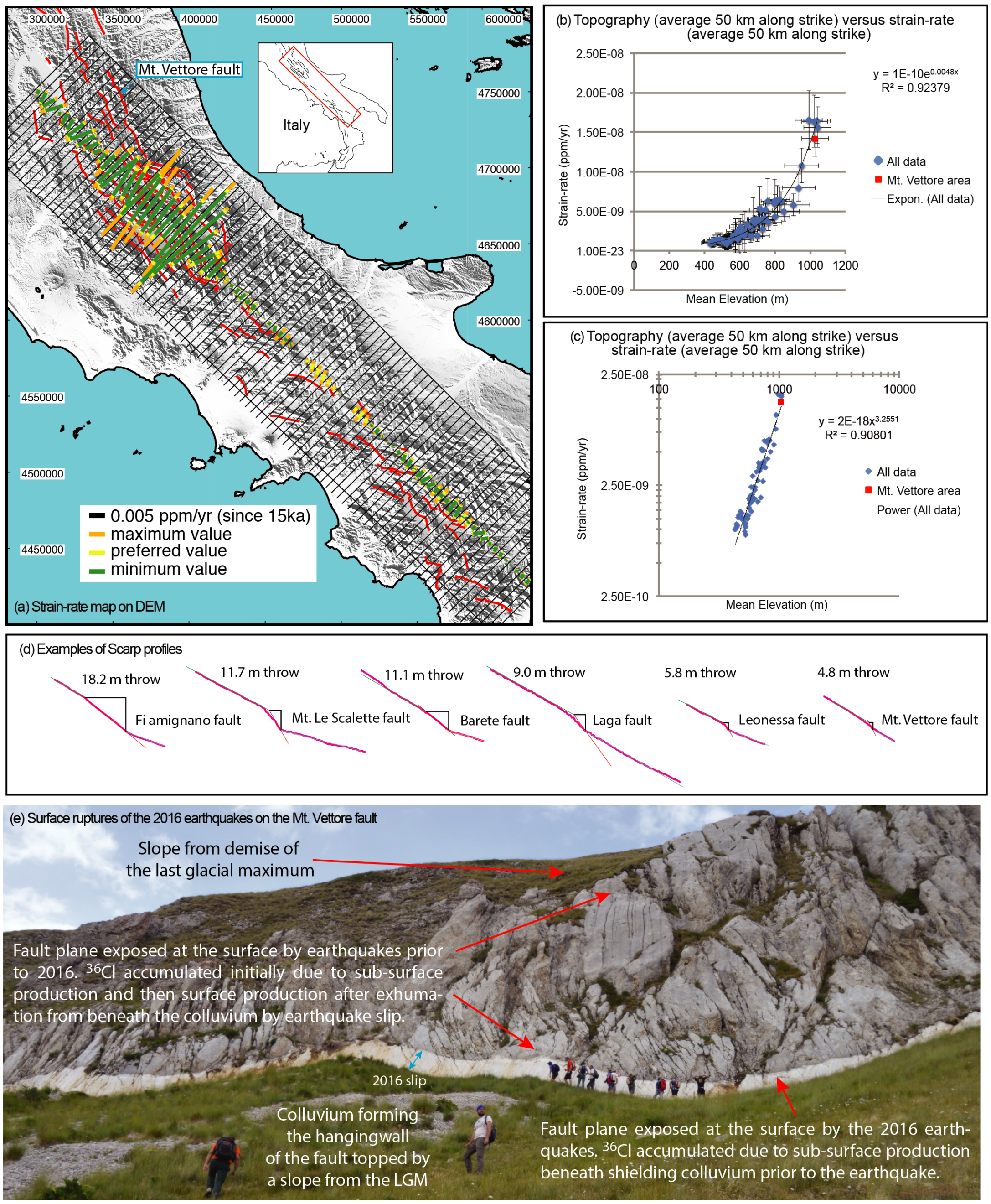

Fig. 1 – Current knowledge of fault and shear zone interaction in the central Apennines. (a) Map showing the spatial variation in principal horizontal strain calculated in 5×90 km boxes (black lines) traversing the Italian Apennines, derived from the directions and magnitudes of faulted-offsets since 15 ±3 ka of landforms dating from the demise of the Last Glacial Maximum, modified and updated from ref.[56] (b) Mean elevation against strain rate from (a), showing a power law correlation between datasets, updated from ref.[3]. (c) Log-log plot of the data presented in (b), showing a power-law relationship with an exponent of ~3.26; the value of this exponent implies that the brittle faults are underlain and driven by viscous shear

zones. (d) Topographic profiles across active fault scarps used in this study. (e) Surface ruptures of the 2016 earthquakes on the Mt. Vettore fault scarp showing how slip on the brittle faults generates surface offsets and hence can be sampled for ^{36}Cl analysis.

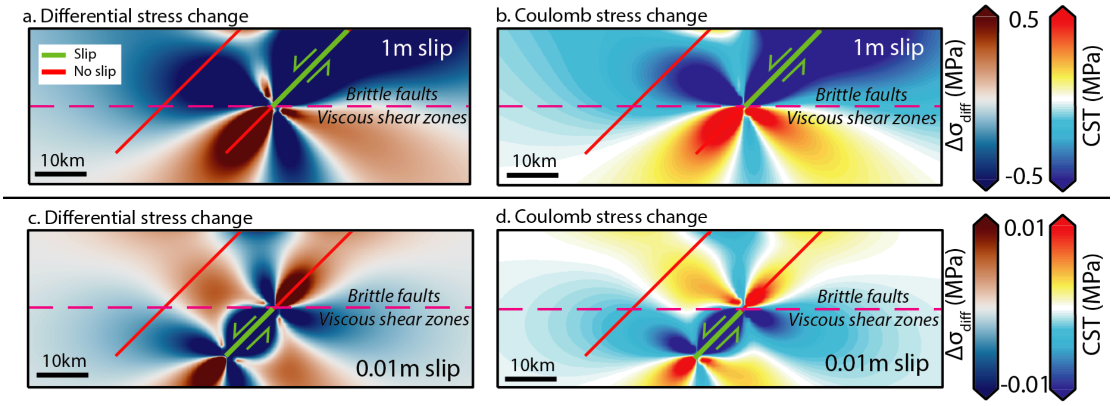

Fig. 2 – Cross-sections showing stress changes produced by slip in normal faulting earthquakes and by slip on underlying shear zones. (a) and (b) show differential and Coulomb stress resulting from a normal faulting earthquake; (c) and (d) show differential and Coulomb stress resulting from slip in a viscous shear zone. Both earthquakes and shear zone slip transfer negative differential stress (a reduction in stress) onto the neighbouring shear zone, so a change in strain-rate on the receiver shear zone is implied.

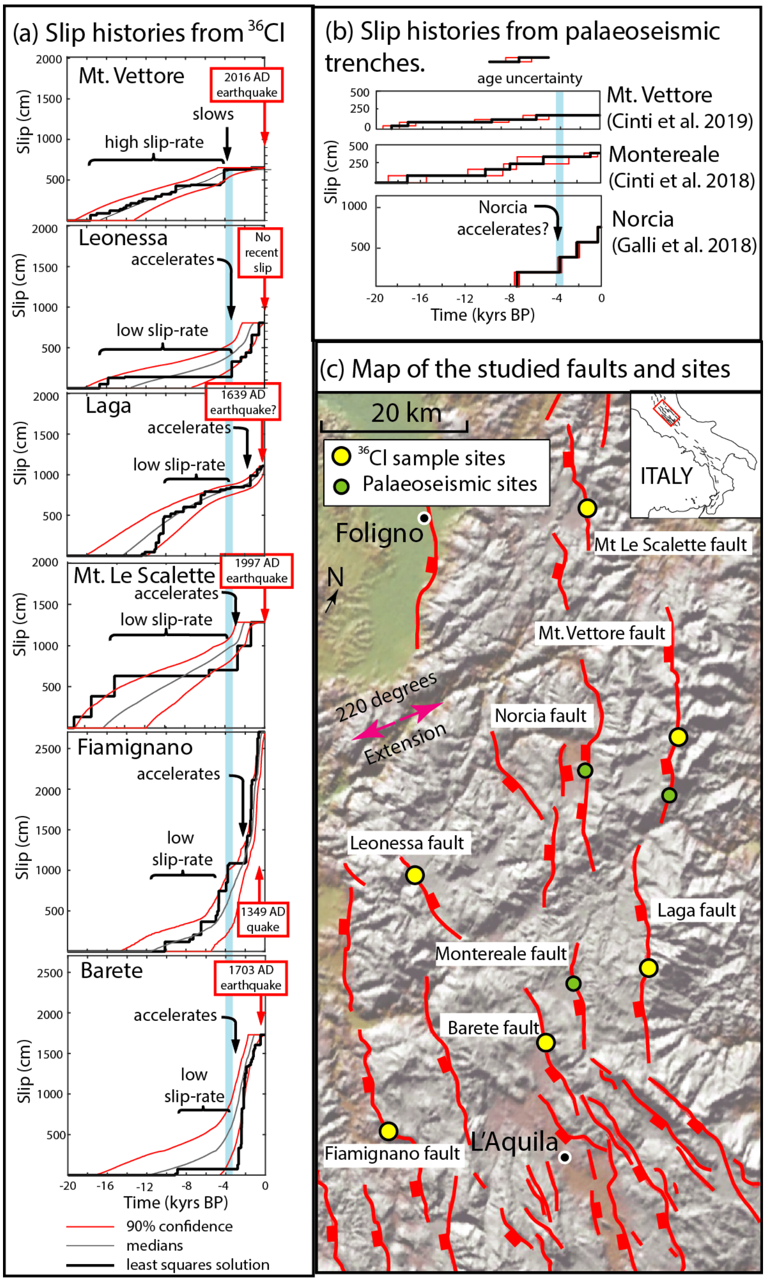

Fig. 3 – Slip histories for the studied active normal faults. (a) Slip histories derived from *in situ* ^{36}Cl cosmogenic exposure data for the six faults studied. At ~3.5 kyrs BP, both the least squares slip histories and 90% confidence curves exhibit convex-upward shapes for the Mt. Vettore fault and convex downward shapes for all the other faults. Concavity indicates that slip-rates change for all the faults at ~3.5 kyrs B.P.; the Mt. Vettore fault slows in activity and has a period of quiescence whilst all the other faults accelerate. (b) Slip histories from other nearby faults from published paleoseismic trenching that broadly agrees with our cosmogenic data. (c) Map showing the locations of the faults studied, ^{36}Cl sample sites and paleoseismic trenches. The change in slip rate evidenced by the ^{36}Cl slip histories is investigated

to determine whether it could be caused by changes in differential stress and hence strain-rate in the underlying shear zones.

(a) Changes in differential stress on shear zones and CST on brittle faults from the combined action of all the other structures

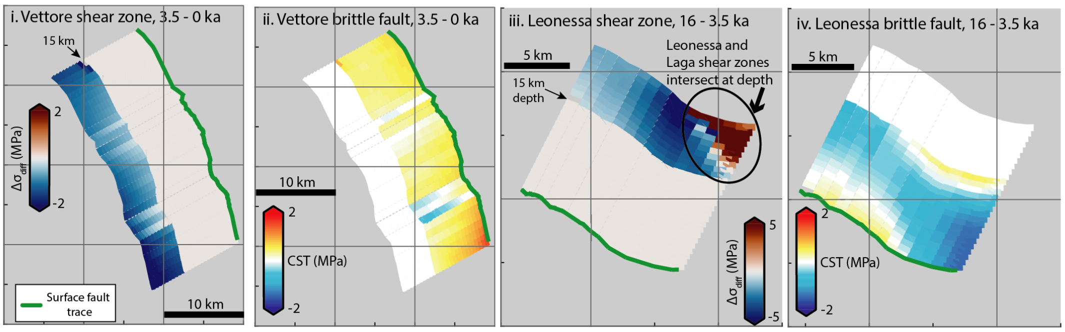

(b) Contributions to changes in differential stress on shear zones from individual structures

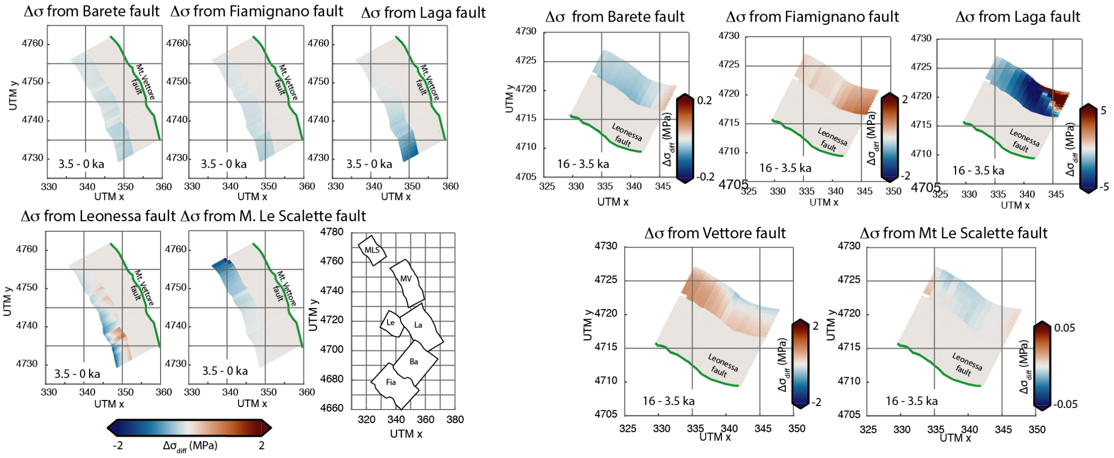

(c) Comparison of measured slip histories and those implied by modelling

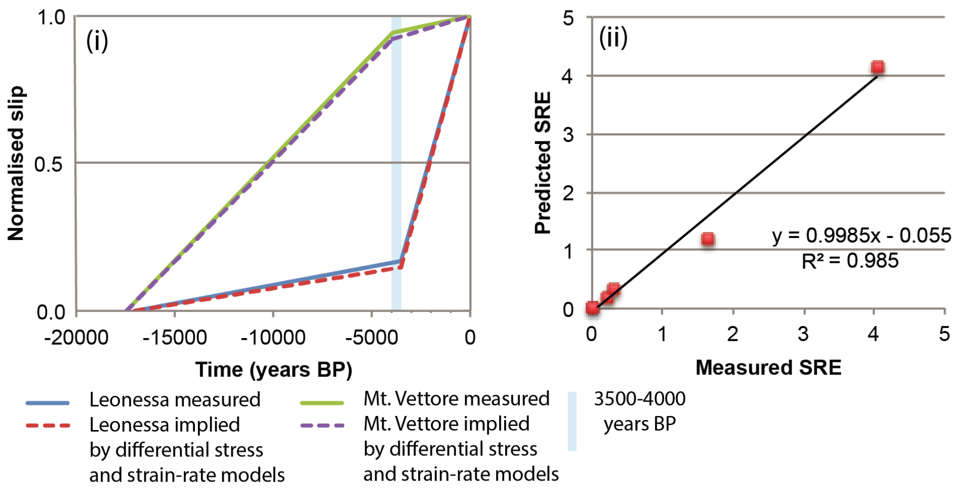

Fig. 4 – Stress changes and effects on slip rates during periods of quiescence for the Mt. Vettore and Leonessa faults. (a) Cumulative changes in differential and Coulomb stress on the Mt. Vettore and Leonessa faults. The periods of quiescence are shown in the slip histories in Fig. 3. (b) Contributions to the cumulative differential stress

from individual neighbouring faults studied with ^{36}Cl analysis, with (a) as the sum of all the values shown in this panel. (c) Comparison between measured slip histories from ^{36}Cl and slip histories inferred from differential stress changes and the quartz flow law. Values are normalised to the total measured slip. Slip Rate Enhancement (SRE) values are calculated relative to the long-term (15 ± 3kyr rate) slip rate, where SRE<1 implies a slowing of slip and a reduction in activity. The similarity between measured and implied slip histories suggests the approach we use, combining stress changes with quartz flow laws, to generate the implied slip histories replicate the natural system.